Supporting Information

Ferguson et al. 10.1073/pnas.1110541108

SI Methods

Bacterial Strains, Cultures, and Sample Preparation. Strains of *Bacillus subtilis* carrying transcriptional fusions with the *gfpmut3* reporter gene were constructed using the pBaSysBioII plasmid designed for high throughput analysis of promoter activities by Live Cell Arrays (1). Integration by a single cross-over event results in the duplication of the promoter region at its homologous chromosomal locus in *B. subtilis* 168 strain (Fig. S2). Protocols for media preparation and cell culture were adapted from Botella et al. (1) and the BaSysBio standardized procedures (http://www.basysbio.eu). Preparation of cell samples and agarose pads for microscopy imaging is described in detail in Ferguson et al. (2). Briefly, cells were harvested from exponentially growing cultures at 37 °C in minimal M9 medium supplemented with either 0.5% glucose (glycolytic conditions) or 0.5% malate (gluconeogenic conditions) as the sole carbon source. Concentrated bacterial aliquots (3 μL) were deposited on M9-agarose (1.5%) pads and covered with a glass coverslip following a procedure allowing the consistent formation of a high-density cell monolayer at the surface.

Two-Photon Scanning Microscopy and Number and Brightness (N&B) Analysis. Cells were imaged on an Axiovert 200M inverted microscope (Zeiss, Germany) equipped with an ISS laser scanning module and an ISS Alba (ISS) with APD detection (SPCM-AQR-15 APD Perkin Elmer). GFP was excited at 930 nm with a femtosecond pulsed infrared Titanium Sapphire laser (Spectra Physics MaiTai, Newport). In the laser scanning module, 930 nm excitation light was expanded to fill the back aperture of a Zeiss Apochromat 63X, 1.4 NA, oil immersion objective. Laser power before injection into the laser scanning module was 15 mW. Infrared excitation light was filtered from the detection path by an E700 SP 2P dichroic filter and a secondary E700 SP 2P filter (Chroma Technologies) placed between the laser scanning module and the detector.

A series of 50 raster scanned 20 μm × 20 μm images of 256 × 256 pixels were recorded with a 50 μs laser dwell time per pixel, chosen to be faster than the GFP diffusion coefficient and to provide statistically relevant photon counts while reducing the effects of photobleaching. Image stacks were analyzed for number and brightness (N&B) values at each pixel taking into account the detector shot noise, using programs written in IDL 6.0 (ITT Visual Information Solutions). A summary of the procedure used in the application of N&B analysis to bacteria is given below, but a detailed explanation of this method, its detection limits and advantages compared to other fluorescence fluctuation-based microscopy methods can be found in (2).

Fluorescence fluctuations (δF) from the average intensity over 50 scans ($\langle F\rangle$) were first calculated at each pixel, providing pixel-based maps of the true (shot noise corrected) molecular brightness, ϵ:

$$\varepsilon(x,y) = \frac{\langle \delta F^2\rangle(x,y) - \langle F\rangle(x,y)}{\langle F\rangle(x,y)} \qquad \textbf{[S1]}$$

The average true molecular brightness $\langle\varepsilon\rangle$ was determined for all of the cells in the field of view using only those central pixels for which the excitation volume ($\mathrm{vol_{ex}}$) is encompassed within the cells. For the rod-shaped *B. subtilis* cells imaged with our two-photon laser microscope, $\mathrm{vol_{ex}}$ has been determined to be 0.07 fL. The spatially averaged true molecular brightness for each field of view allowed for the calculation of the number of molecules, n_{pix} ($/\mathrm{vol_{ex}}$), at each pixel:

$$n_{\mathrm{pix}}(x,y) = \frac{\langle F\rangle^2(x,y)}{\langle \delta F^2\rangle(x,y) - \langle F\rangle(x,y)} \qquad \textbf{[S2]}$$

Then for each cell in the field of view, n_{pix} was averaged over the M pixels situated in an ellipse representing the central 50% of the cell area using a regularized version of Eq. **S7** from Digman et al., (3) to provide the number of molecules in each cell:

$$n_{\mathrm{cell}} = \frac{1}{M}\sum_{j=1}^{M} \frac{\langle F\rangle^2(j)}{\langle \delta F^2\rangle(j)} \frac{\langle\varepsilon\rangle + 1}{\langle\varepsilon\rangle} \qquad \textbf{[S3]}$$

The averaged intracellular concentration of GFPmut3 molecules ($\langle n\rangle_{gfp}$) for a distribution of cells and their intrinsic brightness ($\langle\varepsilon\rangle_{gfp}$) were obtained by correcting the average of the distribution $\langle n_{\mathrm{cell}}\rangle$ for background fluorescence from the *BSB168* receiver strain bearing no *gfp*,

$$\langle n\rangle_{gfp}(\text{molar concentration}) = (\langle n_{\mathrm{cell}}\rangle - \langle n_{\mathrm{cell}}\rangle_{\mathrm{BSB168}})/\mathrm{vol_{ex}}N_A \qquad \textbf{[S4]}$$

$$\langle\varepsilon\rangle_{gfp} = (\langle F_{\mathrm{cell}}\rangle - \langle F_{\mathrm{cell}}\rangle_{\mathrm{BSB168}})/\langle n\rangle_{gfp} \qquad \textbf{[S5]}$$

where N_A is the Avogadro number. The total number of GFP molecules within any individual cell can be obtained by multiplying the concentration **[S3]** by the cell volume, which can be calculated from the images.

Particles number histograms were obtained from measurements on hundreds of different cells for each strain and under each condition tested. Where the background contribution was negligible and the GFP fluorescence signal could be reliably deconvolved, we estimated GFPmut3 intrinsic molecular brightness, $\langle\varepsilon\rangle_{gfp}$, at 0.098 ± 0.024 counts per molecules per 50 μs dwell time ($\sim 2000 \pm 50$ counts per second per molecule). We noted no significant influence of GFP concentration or physiological conditions on the value of $\langle\varepsilon\rangle_{gfp}$ (Fig. S3).

Modeling of Gene Expression from Bacterial Repressible Promoters. We use a two-state promoter model. The two states, denoted as free and bound (or active and inactive) are represented as two binary variables D and DR, respectively. The transitions between the two states are produced by the binding and unbinding of the repressor.

We consider that some of the biochemical reactions depend on the state of the promoter; these reactions are called switched. Switched reactions do not change the state and depend on D, DR. We model this by (formally) considering that switched reactions have D or DR as reactants, but also as products; this formal requirement is just a shorthand and allows us to avoid biochemistry details. The two-state model is based on the hypothesis that the polymerase RNAP concentration is not limiting. Thus, we do not include the concentration of free polymerase among our variables.

Binding and unbinding (or activation and inactivation) of the active repressor R to the DNA-bound RNA-polymerase (D.RNAP) are modeled as reactions of constants k_1^{on} and k_1^{off}, respectively:

$$D + R \underset{k_1^{\text{off}}}{\overset{k_1^{\text{on}}}{\rightleftarrows}} DR \qquad \textbf{[S6]}$$

D takes the values 1 and 0, when the operator site is free or bound by the repressor, respectively. DR is determined by a conservation law:

$$D + DR = 1 \qquad \textbf{[S7]}$$

Transcription initiation followed by the formation of the elongation complex with active, transcribing RNAP (tRNAP) has rate constants k_2 or k_2' depending on repressor being off and on DNA.

$$D \overset{k_2}{\rightarrow} \text{tRNAP} + D \qquad DR \overset{k_2'}{\rightarrow} \text{tRNAP} + DR \qquad \textbf{[S8]}$$

After promoter clearance, the elongation complex transcribes the mRNA leader region with rate constants k_3 or k_3' related to the distance between the promoter and the translation initiation site, and which can be modeled by two switched first order reactions:

$$\text{tRNAP} + D \overset{k_3}{\rightarrow} \text{RBS} + D \qquad \text{tRNAP} + DR \overset{k_3'}{\rightarrow} \text{RBS} + DR \qquad \textbf{[S9]}$$

A switched first order reaction of rate constant k_4 models dissociation of the stalled (active) polymerase from DNA:

$$\text{tRNAP} + DR \overset{k_4}{\rightarrow} DR \qquad \textbf{[S10]}$$

This reaction controls the size of the pool of active stalled polymerase molecules in the tRNAP state, by reducing jamming. A second switched reaction is superfluous and not represented in the free promoter state (considering that this reaction will be dominated by elongation of rate constant k_3 justifies pruning according to the reduction rules presented in Radulescu et al. (4). In our model, and compared to Kierzek et al. (5) [see also Crudu et al. (6)] we pool several states related by rapid transitions and consider that RBS gives rise directly to the ribosome elongating the protein chain, ElRib (rate constant k_6):

$$\text{RBS} \overset{k_6}{\rightarrow} \text{ElRib} + \text{RBS} \qquad \textbf{[S11]}$$

The GFPmut3 variant used in our experiments has been shown to mature within a few minutes (7), therefore we considered that production of folded and matured GFPmut3 (MdGFP) is limited by the step producing the unfolded protein (rate constant k_7). Thus, in our model, we represent only the final folded GFP.

$$\text{ElRib} \overset{k_7}{\rightarrow} \text{MdGFP} \qquad \textbf{[S12]}$$

Both mRNA (RBS) and protein (MdGFP) undergo degradation reactions:

$$\text{RBS} \overset{k_5}{\rightarrow} \emptyset \qquad \textbf{[S13]}$$

$$\text{MdGFP} \overset{k_{\text{deg}}}{\rightarrow} \emptyset \qquad \textbf{[S14]}$$

However, the GFPmut3 fluorescent protein is known to be also very stable (with a lifetime of over 10 hours) and the protein degradation reaction models in fact the dilution resulting from cell growth:

$$k_{\text{deg}} = \log(2)/T, \qquad \textbf{[S15]}$$

where T is the generation time. Reaction **[S13]** gathers several processes. Before the ribosome binds to it, the RBS is unprotected for a short time and degrades with a large constant k_5'. After the ribosome-binding, the RBS degradation is much slower with a constant $k_5'' \ll k_5'$. The effective degradation constant is $k_5 = (1 - p_u)k_5'' + p_u k_5'$ where p_u is the probability to have an unprotected RBS (6). Kierzek et al. (5) uses a full description of the mechanism, but neglects degradation of the protected RBS. The effective degradation in this situation is $k_5 = p_u k_5'$ and needs estimates of both p_u and k_5' to be calculated. The numbers proposed by Kierzek et al. (5) overestimate p_u and lead to very rapid RBS degradation. Here we consider that p_u is very small and take $k_5 = k_5''$. Thus, we do not need values for p_u, k_5' and estimate k_5 directly from the mRNA lifetime (about two minutes in our conditions).

In all cases, the lifetime of the mRNA is much shorter than T (i.e., $k_5 \gg k_{\text{deg}}$).

Parameter Fitting for the Stochastic Model. ***Approximate first moments of the fluctuations.*** The following calculations are important for our fitting procedure.

Let us defined the two switching times:

$$\tau^{\text{on}} = N_A V_o / k_1^{\text{on}} R, \qquad \textbf{[S16]}$$

$$\tau^{\text{off}} = 1/k_1^{\text{off}}, \qquad \textbf{[S17]}$$

that are the times during which the promoter is active and inactive, respectively.

The probability that the promoter is free (active) reads:

$$p = \frac{\tau^{\text{on}}}{\tau^{\text{on}} + \tau^{\text{off}}}. \qquad \textbf{[S18]}$$

Our full model uses a first order reaction mechanism in which the rates constants k_2, k_3, k_4 are two-valued random variables controlled by the repressor. The mean rate constants for the corresponding reactions **S8**–**S10** read:

$$\begin{aligned} \bar{k}_2 &= pk_2 + (1-p)k_2', \\ \bar{k}_3 &= pk_3 + (1-p)k_3', \\ \bar{k}_4 &= (1-p)k_4 \end{aligned} \qquad \textbf{[S19]}$$

The chemical master equation can be used to obtain closed formed equations for the average numbers of molecules at steady-state, in first order reaction mechanisms with deterministic, single-valued rate constants. However, our model has random two-valued constants, and the same method leads to infinite systems of equations for the hierarchy of moments without closure for the first moments. In order to obtain closure, we neglect the correlations between the reaction constant and the number of substrate molecules which reads $\langle kX \rangle = \langle k \rangle \langle X \rangle$ (note that this relation is exact for the zeroth order reaction Eq. **S8** because in this case $X = 1$ and $k = k_2, k_2'$ with probabilities, p and $1 - p$, respectively; in general, this relation can be justified by stochastic averaging when the time scales of the processes k and X are well separated). We obtain the following averaged steady-state equations:

$$\begin{aligned} &\bar{k}_2 = (\bar{k}_3 + \bar{k}_4)\langle \text{tRNAP} \rangle, \qquad \bar{k}_3 \langle \text{tRNAP} \rangle = k_5 \langle \text{RBS} \rangle, \\ &k_6 \langle \text{RBS} \rangle = k_7 \langle \text{ElRib} \rangle = k_{\text{deg}} \langle \text{MdGFP} \rangle \end{aligned} \qquad \textbf{[S20]}$$

Using Eqs. **S18** and **S20**, we obtain an analytic approximation for the average MdGFP:

$$\langle \mathrm{MdGFP} \rangle = \frac{\bar{k}_2}{k_{\deg}} \frac{\bar{k}_3}{\bar{k}_3 + \bar{k}_4} \frac{k_6}{k_5}. \quad \textbf{[S21]}$$

Approximate second moments of the fluctuations. Considering that a burst is produced each time the repressor unbinds (this hypothesis is valid if the mRNA burst size defined as the product $k_2\tau^{\mathrm{on}}$ is sufficiently strong), the frequency of bursts (average number of bursts during the time, $T/\log(2) = 1/k_{\deg}$) is simply:

$$a = \frac{1}{k_{\deg}(\tau^{\mathrm{off}} + \tau^{\mathrm{on}})} \quad \textbf{[S22]}$$

In the bursting regime, the bursting frequency a, the burst amplitude b, the mean $\langle \mathrm{MdGFP} \rangle$ and the variance Var(MdGFP) of the number of proteins satisfy the following approximate Gamma distribution relations (the Gamma approximation proposed by Friedman et al. (8) is correct under conditions (τ^{on} must be much shorter than τ^{off} and the burst size sufficiently large) specified in Crudu et al. (6):

$$a = \langle \mathrm{MdGFP} \rangle^2 / \mathrm{Var}(\mathrm{MdGFP}) \quad \textbf{[S23]}$$

$$b = \mathrm{Var}(\mathrm{MdGFP}) / \langle \mathrm{MdGFP} \rangle \quad \textbf{[S24]}$$

From Eqs. **S21**–**S24** we can obtain an approximation for the second moment of the steady-state distribution of the protein numbers:

$$\mathrm{Var}(\mathrm{MdGFP}) = k_{\deg}(\tau^{\mathrm{off}} + \tau^{\mathrm{on}}) \left[\frac{\bar{k}_2}{k_{\deg}} \frac{\bar{k}_3}{\bar{k}_3 + \bar{k}_4} \frac{k_6}{k_5} \right]^2 \quad \textbf{[S25]}$$

To summarize, in gene networks, the type and the amplitude of steady-state fluctuations depend on the relations between the time scales of the system. We emphasized two switching times, $\tau^{\mathrm{on}} = N_A V_o / k_1^{\mathrm{on}} R$ (with V_0 the cell volume and N_A the Avogadro's number) and $\tau^{\mathrm{off}} = 1/k_1^{\mathrm{off}}$, corresponding to the periods during which the active repressor R is unbound and bound to the DNA, respectively. Another important time scale is the lifetime of the mRNA, $\tau_5 = 1/k_5$. Depending on the relations between these time scales, our model can have different stochastic regimes: Poissonian, bursting, and telegraph noise regime. The Poissonian regime corresponds to fast switching, when $\tau^{\mathrm{on}} + \tau^{\mathrm{off}} \ll \tau_5$. Bursting means that the promoter has very strong activity during a very short period, $\tau_b = \tau^{\mathrm{on}} \ll \tau_5$ that is followed by a longer inactivity period, $\tau^{\mathrm{off}} \gg \tau^{\mathrm{on}}$, whereas these periods are equivalent for telegraph noise. In the case of bursting, the burst frequency is given by Eq. **S22** if a burst occurs each time the repressor unbinds. If the number of mRNA per burst is small (the mean value $k_2\tau^{\mathrm{on}}$ is small) then the probability to have no burst when the repressor unbinds is not negligible. In this case the burst frequency Eq. **S22** should be corrected by the factor $1 - \exp(-k_2\tau^{\mathrm{on}})$ smaller than one, which is the probability to have at least one transcript when repressor unbinds. The Eq. **S25** would change accordingly. Because we use the approximation only as an initial guess, we did not apply this correction.

Parameter optimization. We consider that, for each of the two carbon sources used in this study, the bacteria population had enough time to adapt and to reach exponential growth. Accordingly, distributions of gene expression can be considered to be at steady-state. The experimental histograms have to be compared to the theoretical steady-state probability densities. The latter are solutions of the stationary master equation for the above model and depend on several model parameters μ and the conditions $\alpha \in [1,2]$ (two nutrient conditions). The numbers of molecules predicted by the stochastic dynamics of the model in the bacterium volume V_0 were divided by a factor 10 to cope with the difference between the observation volume (0.07 fl) and the bacterium volume (approximately 0.7 fl). An independent random variable has been added to the resulting numbers to account for the fluorescence background (of mean 17.48 and variance 14.51 in the observation volume of 0.07 fl).

Let $\{p_i^{\exp}(\alpha)\}_{1 \le i \le N}$ be the experimental histogram computed with bin centers n_i and $\{p_i(\mu;\alpha)\}_{1 \le i \le N}$ be the theoretical density estimated at n_i. We search for parameters μ minimizing the following objective function:

$$f(\mu;\alpha) = \sum_{\alpha=1}^{2} \sum_{i=1}^{N} (p_i(\mu;\alpha) - p_i^{\exp}(\alpha))^2. \quad \textbf{[S26]}$$

For this complex model, we do not posses analytical solutions of the master equations. Therefore, comparison between model and data, as well as parameter regression should rely on extremely time consuming numerical simulations by the Gillespie algorithm. Two improvements of this brute force strategy allowed us to reduce the computation time.

Averaging. The main problem of the Gillespie algorithm is fast unbroken cycles (see ref. 6) that lead to expensive computation. Note that multiscale systems of chemical reactions may contain fast reactions that are the cause of expensive computation. For example, the total number of simulated reactions through a rapid chain is small, because the source is rapidly exhausted. A fast unbroken cycle is a cycle containing fast reactions and having non-negligible mass at steady-state. Unbroken means that whenever there are reactions getting mass out of the cycle, these are slower than reactions recirculating the mass within the cycle. Fast unbroken cycles are sources of expensive computation because they fire fast reactions continuously and recyle molecules. A simple solution to accelerate simulation of such cycles is averaging, consisting in replacing the cycling fast variables by their average values. In the repressed state of the promoter P_{cggR}, the fast cycle, RNAP → tRNAP, tRNAP → RNAP, produces rapid oscillations of tRNAP around its average value. In the unrepressed state of the promoter P_{cggR}, and all the time for the promoter PgapB, this cycle is broken by the faster reaction

$$\mathrm{tRNAP} \rightarrow \mathrm{RBS} + \mathrm{RNAP}$$

(not active during repressed state). Averaging in this case means simply replacing tRNAP with its average value computed with Eq. **S20**. Because the promoter is almost all the time repressed, this leads to a drastic reduction of the simulation time in the case of P_{cggR}. Simulation of PgapB does not have this problem and is sufficiently fast. The gain in execution speed allowed us to generate a sufficiently large number of samples needed to estimate the stationary probability density.

Using analytical approximations for the moments of the distribution. The second improvement allows us to reduce our optimization problem to a local search. Starting with analytical approximations for the first two moments of the theoretical distribution, Eqs. **S21**, **S25**, we fix some parameters to generic values, and fit others from the first two moments of the experimental histograms under different conditions. This has been done according to the following procedure.

1) Choose values for invariant parameters. Some parameters depend only on the GFP reporter and do not depend on the promoter or carbon source.

- k_5, (degradation of mRNA molecules) were chosen as already described (2 min for the lifetime of mRNA $\tau_5 = 1/k_5$, averaging between unprotected (5) and ribosome protected mRNA and reasonable for our growth conditions).
- k_6, (ribosome-binding and translation initiation to the RBS) is taken from Kierzek et al. (5) assuming fast binding by saturating ribosomes, and 0.5 s^{-1} for RBS clearance.
- k_7 (translation, folding and maturation of the GFP) taken to be 1–10 min, as we observe GFP fluorescence in one minute after induction and the halt of the increase in GFP signal between 1–10 minutes after administration of a ribsome poisoning antibiotic. The fit was effectuated with 1 min; we have checked that an increase of this time by a factor 10, modifies the fitted parameters by less than 5%.
- $k_{\rm deg}$, (degradation of GFP) is calculated from Eq. **S15** using an average generation time of 70 min as experimentally determined.

2) Choice of parameters that do not depend on carbon source, but depend on the promoter.

- k_2' (transcription initiation and promoter clearance) was considered very small for P_{gapB} (CcpN is thought to interact with RNAP and impede initiation as described in the main text), namely $k_2' \ll pk_2$, and equal to k_2 for P_{cggR}.
- k_3 (transcription of the mRNA leader region from the promoter to the RBS) was estimated using the rate of polymerase movement (30–45 nucleotides per sec at 37 °C (9) and the length between the transcription start and the RBS (about 95 bp in case of P_{cggR}, 45 bp in case of P_{gapB}).
- k_3' was considered very small for CggR because of the roadblock exerted on the transcribing RNAP, namely $k_3' \ll pk_3$, and equal to k_3 for GapB (no roadblock).
- k_4 (dissociation of the transcribing RNAP) was chosen an order of magnitude smaller than k_3. Smaller values would produce crowding, therefore we need $k_4 \gg pk_3$.

Parameter fit. The parameters $k_2, k_1^{\rm on}, k_1^{\rm off}$ were fitted from data, as follows:

We provide some range for the parameter k_2, 0.5–1 for P_{cggR} and 0.001–1 for P_{gapB}. Eq. **S21** allows finding p (probability that the promoter is free/active) from the average expression. Interestingly, this was found small for the two promoters in all conditions. Together with the condition $k_4 \gg pk_3$, this finding justifies the following simplified expressions, resulting from Eqs. **S18**, **S21**, and **S25** when p is small:

$$p = \tau^{\rm on} k_1^{\rm off}. \qquad \textbf{[S27]}$$

$$N_{gapB} = \frac{\tau^{\rm on}k_1^{\rm off}}{k_{\rm deg}}\frac{k_6k_2}{k_5}, \qquad N_{cggr} = \frac{\tau^{\rm on}k_1^{\rm off}}{k_{\rm deg}}\frac{k_3k_6k_2}{k_4k_5} \qquad \textbf{[S28]}$$

$$a = \frac{k_1^{\rm off}}{k_{\rm deg}} \qquad \textbf{[S29]}$$

$$b_{gapB} = \tau^{\rm on}\frac{k_6k_2}{k_5}, \qquad b_{cggr} = \tau^{\rm on}\frac{k_3k_6k_2}{k_4k_5} \qquad \textbf{[S30]}$$

where N_{gapB}, b_{gapB} are the average expression and burst amplitude for PgapB, PcggR respectively.

From the experimental values of a and Eq. **S29** we can directly estimate the parameter $k_1^{\rm off}$. Once this found we can use Eq. **S28** to find $\tau^{\rm on}$ for several values of k_2. By numerical tests we found that Eq. **S28** is rather accurate, but Eq. **S29** and Eq. **S30** are less accurate (the reason is the small number of mRNA per burst in the repressed conditions; see below). Next, we used Gillespie simulations (instead of the approximated formulas) to fit the parameters $k_1^{\rm off}$, $\tau^{\rm on}$ and k_2. Starting with preliminary estimates as initial guess, we searched for the best fit of experimental average and Fano factor under the two conditions. For this stage, Gillespie simulations estimate the first two moments, which is less time costly than estimating the full distribution.

The result of the parameter relaxation for P_{gapB} is shown in Fig. S4*A*. We can notice from Eq. S28 that given k_2 and the mean expression, the parameters $k_1^{\rm off}$, $\tau^{\rm on}$ are inversely proportional. In order to increase the Fano factor b, $\tau^{\rm on}$ should increase and $k_1^{\rm off}$ should decrease by the same factor. However, in repressed states, Eq. **S30** overestimates the sensitivity of the Fano factor on $\tau^{\rm on}$ and $k_1^{\rm off}$. It is possible, that once the average is fitted, which fixes the product $\tau^{\rm on}k_1^{\rm off}$, the optimization procedure uses large changes to $\tau^{\rm on}$ in order to fit the Fano factor. This means that, although the product $\tau^{\rm on}k_1^{\rm off}$ is accurate, the absolute values of $\tau^{\rm on}$ and $k_1^{\rm off}$ could have large errors in repressed conditions, especially for P_{gapB} where repression is drastic. Furthermore, k_2 must be chosen to fit both repressed and permissive conditions. Although the choice in the imposed range can be arbitrary for permissive conditions, it is not so for the repressed conditions. Indeed, in the latter conditions, the Fano factor depends less on $k_1^{\rm on}$ and more on k_2, which imposes the tuning of k_2.

After this stage we obtain a full set of parameters that fit the first two moments of the expression distribution. Further refinement uses the objective function Eq. **S26** and needs estimates of the distribution. The refined parameter values are given in Table S1.

To conclude, the discussion shows that parameters $\tau^{\rm on}$, $k_1^{\rm off}$, k_2, k_3, k_4, k_5, k_6, $k_{\rm deg}$ are critical. Remaining parameters are noncritical and do not need to be known with precision. For instance k_7 is noncritical. Similarly, the value of k_3 for P_{gapB} is noncritical.

Although the number of critical parameters may seem large, a number of these can be compacted into a single effective parameter such as $\frac{k_2k_3k_6}{k_4k_5k_{\rm deg}}$ for P_{cggR}, or $\frac{k_2k_6}{k_5k_{\rm deg}}$ for P_{gapB}. A change of this effective parameter will change the absolute values of the fitted parameters but not their relative changes from one condition to another. As a consequence, although choices for some critical parameters may need changes from the generic values that we used, we can trust the relative variations of the fitted parameters from repressed to permissive conditions.

Distribution and moments from Gillespie simulations. Gillespie simulations generate trajectories $(t_i,X_i), i \in [1,N]$, where t_i, X_i represent times when a reaction happens and numbers of protein molecules after the reaction, respectively. The length of these trajectories is several thousands of generation times. By the ergodic theorem for Markov processes we can use long trajectories to estimate state probabilities by the average time spent in a state. Similarly, the moments of the steady-state distribution are estimated as follows:

$$\langle X\rangle = \frac{1}{t_N - t_1}\sum_{i=1}^{N} X_i(t_{i+1} - t_i) \qquad \textbf{[S31]}$$

$$\langle X^2\rangle = \frac{1}{t_N - t_1}\sum_{i=1}^{N} X_i^2(t_{i+1} - t_i) \qquad \textbf{[S32]}$$

$$\mathrm{Var}(X) = \langle X^2\rangle - \langle X\rangle^2 \qquad \textbf{[S33]}$$

In order to estimate the steady-state distribution, we have chosen to resample (by interpolation) the trajectory $(t_i,X_i), i \in [1,N]$, by using a constant time step. The result is a vector $(X_i'), i \in [1,M]$, representing realizations of the steady-state variable X. We add

to this an independent vector $(B_i), i \in [1,M]$, representing the background (this was generated using a gamma distribution with parameters given by the background average and variance). The vector $(X'_i + B_i), i \in [1,M]$, is used to estimate the steady-state distribution that is compared to the experimental histograms.

1. Botella E, et al. (2010) pBaSysBioII: An integrative plasmid generating *gfp* transcriptional fusions for high-throughput analysis of gene expression in *Bacillus subtilis*. *Microbiology* 156:1600.
2. Ferguson ML, et al. (2011) Absolute quantification of gene expression in individual bacterial cells using two-photon fluctuation microscopy. *Anal Biochem*419:250–259.
3. Digman MA, et al. (2008) Mapping the number of molecules and brightness in the laser scanning microscope. *Biophys J* 94:2320–2332.
4. Radulescu O, et al. (2008) Robust simplifications of multiscale biochemical networks. *BMC Syst Biol* 2:86.
5. Kierzek AM, Zaim J, Zielenkiewicz P (2001) The effect of transcription and translation initiation frequencies on the stochastic fluctuations in prokaryotic gene expression. *J Biol Chem* 276:8165–8172.
6. Crudu A, Debussche A, Radulescu O (2009) Hybrid stochastic simplifications for multiscale gene networks. *BMC Syst Biol* 3:89.
7. Cormac BP, Valdivia RH, Falkow S (1996) FACS-optimized mutants of the green fluorescent protein (GFP). *Gene* 173:33.
8. Friedman N, Cai L, Xie XS (2006) Linking stochastic dynamics to population distribution: An analytical framework of gene expression. *Phys Rev Lett* 97:168302.
9. Golding I, et al. (2005) Real-time kinetics of gene activity in individual bacteria. *Cell* 123:1025–1036.

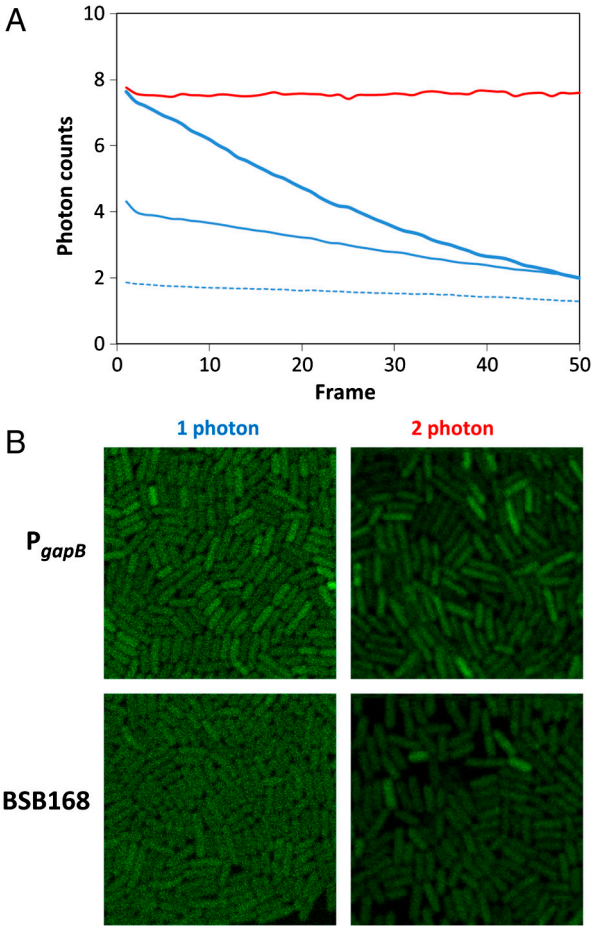

Fig. S1. Comparison of 1-photon vs 2-photon scanning microscopy of live bacterial cells expressing *gfpmut3* promotor fusions. (*A*) Mean fluorescence intensity decrease over 50 scans of immobilized *B. subtilis* cells expressing P_{gapB}*gfpmut*3 under malate and imaged using our 2-photon set-up (red line) or a confocal 1-photon microscope (blue lines) at different laser power (thick line, 0.5%; thin line, 0.2%; dotted line 0.1%). For each acquisition, 50 frames of 20×20 μm (256×256 pixels) were recorded using a laser dwell time of 50 μs. A Zeiss LSM780 confocal microscope was used in photon-counting mode, using an excitation wavelength of 488 nm and a GaAs-P detector witha 481–551 nm emission band pass. In the two-photon mode, GFP was excited at 930 nm with a femtosecond pulsed infrared laser at 15 mW as desribed in *Materials and Methods*. Severe photobleaching is observed in the 1-photon mode except at very low laser power (0.1%), whereas no photobleaching is observed under the conditions used in this study for two-photon scanning microscopy. (*B*). Fluorescence images of the strongly repressed P_{gapB}*gfpmut*3 transriptional fusion strain grown on glucose and of the BSB168 receiver strain carrying no *gfp*. The same cell samples were imaged with the confocal microscope using the lowest laser power (0.1%) or with the 2-photon microscope with the addition of a filter band pass 525/70 (Chroma). Images of the total fluorescence recorded over 50 scans are shown using the same brightness and contrast levels. The auto fluorescence background level observed in the receiver strain is lower in the two-photon mode, revealing cell-cell variations hardly visible in the one-photon mode.

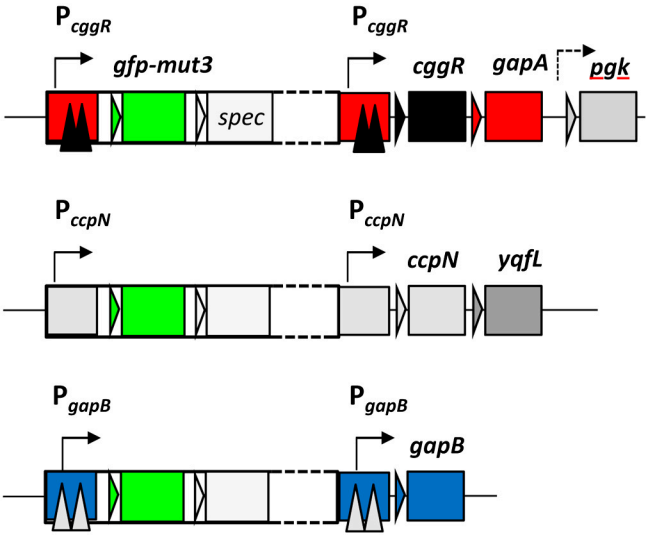

Fig. S2. Organization of the *B. subtilis* chromosomal region carrying the gfpmu3 promoter fusions used in this study. DNA fragments of about 400 bp comprising the promoter regions are fused to the 5′ end of the *gfpmut3* coding sequence (green box) preceded by an optimized ribosome-binding site (RBS, green triangle) ensuring that all the steps yielding to GFP production past the synthesis of the RBS are identical. Integration of the pBaSysBioII derivatives (1) carrying the *gfp* transcriptional fusions and a spectinomycin resistance gene (*spec*) results in the duplication of the promoter and regulatory region. In case of the *gapA* operon (top schematic) induced under glycolytic conditions, the double operator site recognized by the CggR repressor (black triangles) is located between the promoter sequence for transcription start (black arrow) and the *cggR* gene, the first gene of this auto-regulated operon. An alternative promoter (dotted arrow) allows for the weak constitutive expression of the four downstream glycolytic genes of the *gapA* operon (beginning with *pgk*, as shown). Middle schematic shows the unregulated *ccpN* promoter, from which both CcpN and its negative regulator, YqfL are expressed. CcpN represses the expression of the gluoconeogenic genes *gapB* (bottom schematic) and *pckA*, one of its tandem operator sites (duplicated gray triangles) overlapping with the promoter sequence. Organization of the *pckA* promoter fusion is very similar to that of *gapB*.

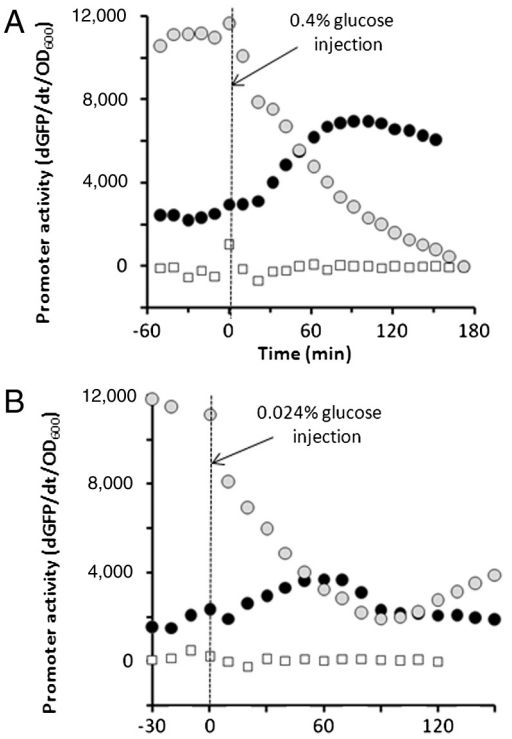

Fig. S3. Promoter activity profiles monitored by LCA of P_{cggR} and P_{gapB} during a nutritional shift. Fluorescence changes (*A*) and growth curve (*B*) of the reference strain BSB168 (white squares) and the P_{cggR}-*gfpmut3* (black circles) or P_{gapB}-*gfpmut3* (gray circles) fusion strains were monitored in 96-well microplates (CELLSTAR Greiner Bioone). Cells were grown to exponential phase at 37 °C in 100 μL of M9 synthetic medium supplemented with 0.4% malate as a carbon source. At the time indicated by a dotted line, glucose was added to cultures growing exponentially on M9-malate, at a final concentration of 0.4%. LCA measurements and calculation of promotor activities were performed as described in Botella et al. (1).

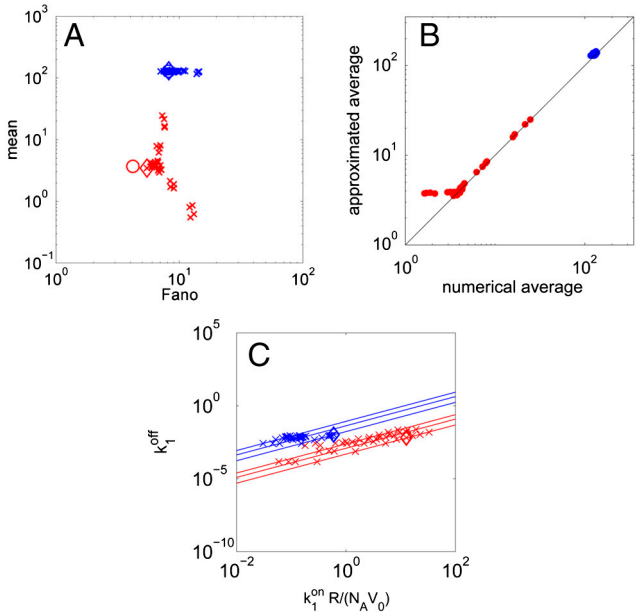

Fig. S4. Parameter fit for P_{gapB} in glucose (red) and malate (blue) conditions. Starting from preliminary estimates the parameters were relaxed to fit the experimental average and Fano factor associated to the observed numbers distribution as shown in Fig. 4*C* (*A*) circles are experimental values, diamonds values for optimal parameters, crosses, various relaxation steps. (*B*) The approximate formula for the average expression Eq. **S21** is compared to the numerical average. (*C*) Values of the parameters at various relaxation steps. Diamonds are optimal parameters. Along the lines the average expression is constant, various lines correspond to different values of k_2 (0.04, 0.08, 0.2).

Table S1. Estimated and fitted parameters used for modeling P_{cggR} and P_{gapB} promoter activity

			Estimated or fitted value [s^{-1}]†			
			P_{cggR}		P_{gapB}	
Reaction*		Rate constant	malate	glucose	malate	glucose
$D + R \rightarrow DR$	Binding of repressor molecules to operator DNA	$k_1^{on} R/(N_A V_o)$‡	5.4 (0.1–10)	11.2 (1–100)	0.6 (0.1–10)	12.7 (0.1–10)
$DR \rightarrow D + R$	Dissociation of the repressor from operator DNA	k_1^{off}	0.00085 (0.0001–0.1)	0.0116 (0.005–5)	0.01 (0.01–1)	0.007 (0.01–1)
D + RNAP → D + tRNAP	Transcription initiation and promoter clearance	k_2	0.6 (0.5–1)	0.6 (0.5–1)	0.2 (0.001–1)	0.2 (0.001–1)
DR + RNAP → DR + tRNAP	id as above in the presence of the repressor	k_2'	0.6 (0.5–1)	0.6 (0.5–1)	<0.001 (0.00001–1)	<0.00002 (0.00001–1)
D + tRNAP → D + RBS	Transcription of the mRNA leader region (from promoter to RBS)	k_3	0.15	0.15	0.33	0.33
DR + tRNAP → DR + RBS	id as above in the presence of the repressor	k_3'	<0.00002 (0.00001–0.01)	<0.0001 (0.00001 0.01)	0.33	0.33
DR + tRNAP → DR + RNAP	Dissociation of RNAP	k_4	0.01 (0.0001–0.01)	0.01 (0.0001–0.01)	≪0.33	≪0.33
RBS → Ø	Degradation of mRNA molecules	k_5	0.008	0.008	0.008	0.008
RBS → ElRib + RBS	Ribosome-binding and translation initiation	k_6	0.5	0.5	0.5	0.5
ElRib → MdGFP	Translation, folding and maturation of GFP	k_7	0.015	0.015	0.015	0.015
MdGFP → Ø	Degradation of matured GFP	k_{deg}	0.000165	0.000165	0.000165	0.000165

*D, operator DNA; R, repressor molecule; RNAP, RNA-polymerase; tRNAP, transcribing RNAP; RBS, mRNA molecule with ribosome-binding site; ElRIB, elongating ribosome; MdGFP, matured green fluorescent protein; Ø, degraded molecule.

†Estimated or fitted values of the rate constants used for the simulation of transcriptional activities from the P_{cggR} or P_{gapB} promoters at steady-state in *B. subtilis* cells grown on malate or glucose. Values obtained by fitting the experimental distribution data (Fig. 4*C*) are underlined, with their acceptable estimated range indicated in parenthesis. Explanations and references for the choice of the invariant and fitted parameters are given in *SI Text*.

‡N_A: Avogadro's number; V_0: average volume of the bacterial cells (0.7 fL).